4

Multipoint Analysis of Electric Currents in Geospace Using the Curlometer Technique

M. W. Dunlop[1,9], S. Haaland[2], X-C. Dong[1], H. R. Middleton[3], C. P. Escoubet[4], Y.-Y. Yang[5], Q.-H. Zhang[6], J-K. Shi[7], and C. T. Russell[8]

ABSTRACT

Four-point magnetic field measurements in space allow estimates of the electric current density through the curlometer technique, which estimates electric current density from Ampère's law, and is relevant to the magnetosphere and surrounding regions, which contain high conductivity plasma. Knowledge of spacecraft separations, magnetic field measurement accuracy, and the form of the current structures sampled (e.g., relative scale size) limits the accuracy of the method. Despite these conditions of application, in many regions of the magnetosphere it has been shown to be robust and reliable. A number of studies have applied the method successfully such as: the ring current; the magnetotail current sheet; the magnetopause currents, and field aligned currents, as well as to other current structures (e.g., flux tubes). Where time stationarity and other special assumptions can be made, or where the spacecraft configuration is highly irregular or less than four spacecraft are available, the method can still be applied to obtain partial components of the current. We discuss the application of the curlometer technique to the four-point observations from the Cluster mission in terms of its adaptability and performance (including the lessons learned) and illustrate its use with recent data from the MMS mission, which covers a much smaller spatial regime.

[1] *Space Science Institute, School of Astronautics, Beihang University, Beijing, China*

[2] *Birkeland Centre for Space Science, University of Bergen, Norway; Max-Planck Institute for Solar Systems Research, Göttingen, Germany*

[3] *ESA/ESAC, Villanueva de la Cañada, Madrid, Spain*

[4] *ESA/ESTEC, Noordwijk, The Netherlands*

[5] *Key Laboratory of Crustal Dynamics, China Earthquake Administration, Beijing, China*

[6] *Institute of Space Sciences, Shandong University, Weihai, China*

[7] *NSSC, Chinese Academy of Sciences, Beijing, China*

[8] *UCLA, Los Angeles, California, USA*

[9] *RAL Space, STFC, Chilton, Oxfordshire, UK*

4.1. INTRODUCTION: CURRENTS IN GEOSPACE

As shown in Chapter 2, a wide range of currents permeates many regions of space and, in particular, currents are ubiquitous in the Earth's magnetosphere (see Fig. 4.1), supporting both large-scale and small-scale plasma structures (in the form of sheets, tubes, and other structures) and connecting different regions (as in the case of field-aligned currents). In the terrestrial magnetosphere, pronounced current systems include the ring current (see Chapter 7), the cross-tail current sheet (see Chapter 10), and the magnetopause current (see Chapter 13). Field-aligned currents (FACs, see section IV of this volume)

Electric Currents in Geospace and Beyond, *Geophysical Monograph 235*, First Edition.
Edited by Andreas Keiling, Octav Marghitu, and Michael Wheatland.

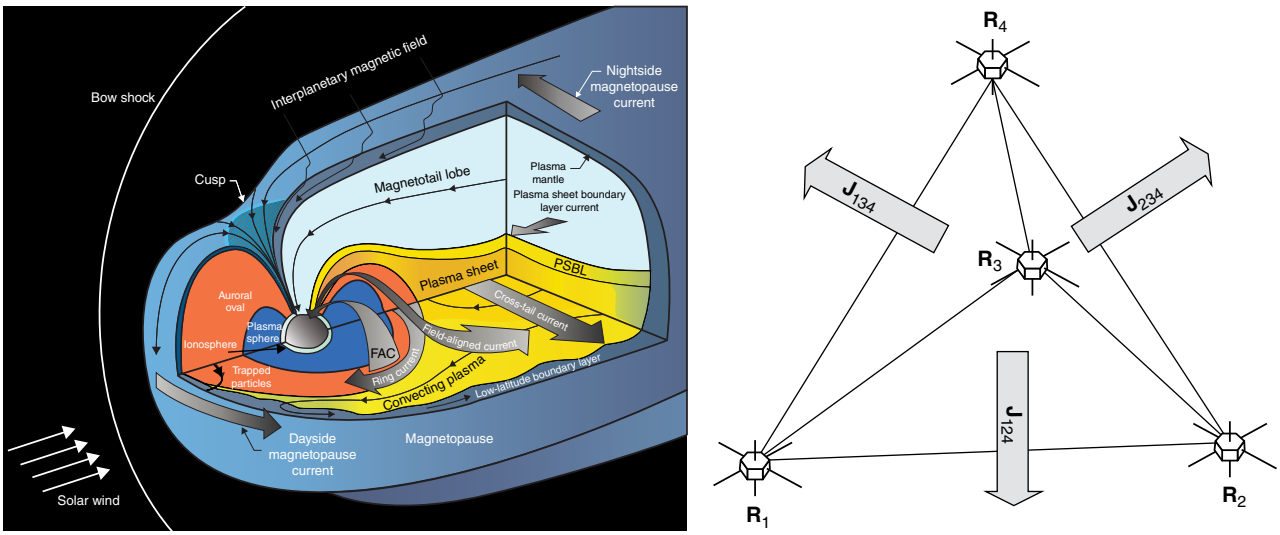

Figure 4.1 (Left) Depiction of the large-scale currents in the Earth's magnetosphere (adapted from *Kivelson and Russell* [1995]), and (right) the curlometer concept (after *Dunlop et al.* [1988]).

connect the collisionless plasma regime in the magnetosphere with the Earth's collision-dominated ionosphere. Other currents may exist in the plasma sheet boundary layer and within the cusp boundaries, and within transient structures such as opened flux tubes caused by magnetic reconnection.

Currents are set up by differential motion of charged particles. In simple terms, the current density can thus be derived from density and velocity moments of ions and electrons:

$$\mathbf{J} = \sum \mathrm{q} n_s \mathbf{V_s} \sim \mathrm{q} n \left(\mathbf{V_i} - \mathbf{V_e} \right) \tag{4.1}$$

where $n = n_i = n_e$ is the density (assuming quasi neutrality), V_i is the ion bulk velocity and V_e is the corresponding electron bulk velocity. In practice, this approach is difficult and will require particle detectors with identical characteristics for all ion species and electrons in terms of angular resolution, energy ranges, sensitivity, and calibration. Since particle moments will have to be based on 3D particle velocity distribution functions, measurements often rely on spacecraft spin (and thus have limited time resolution) or arrays of detectors to obtain full coverage. Examples, using particle moments from the Cluster satellites [*Escoubet et al.*, 2001] can be found in publications by, for example, *Henderson et al.* [2008] and *Petrukovich et al.* [2015]. Recent results from the Magnetospheric Multiscale (MMS) mission [*Burch et al.*, 2016] benefit from far better time resolution, and sampling at much smaller spatial separations, and will provide new opportunities to use particle moments to estimate currents (see section 4.3.2).

In space, either currents are also sources of magnetic fields or they modify existing magnetic fields (e.g., the Earth's dipole magnetic field). The relation between currents and magnetic field perturbations is given by Ampère's law (for highly conducting plasmas where quasi neutrality typically applies, the displacement current, $\mu_0 \varepsilon_0 \partial E / \partial t$, where E is the electric field, can be neglected in the corresponding Maxwell equation [*Russell, et al.*, 2016]):

$$\mu_0 \mathbf{J} = \mathbf{curl}\left(\mathbf{B}\right)$$

This relation enables us to derive the strength and orientation of currents directly from the magnetic field and its gradients without any particle measurements (or to compare between the two estimates). Magnetic fields can typically be measured with higher accuracy and higher time resolution than particle moments.

Multiple spacecraft flying in formation (a constellation) allow the curlometer technique, using Ampère's law above, to estimate the electric current density from **curl(B)**, suitable for the magnetosphere and surrounding regions, which contain plasma with high conductivity. The method was introduced to utilize four-point measurements in space; anticipating the realization of the four-spacecraft Cluster mission [*Escoubet et al.*, 2001], which began full science operations in February 2001 and provided the spatial measurements from which a linear calculation of the curl of the magnetic field can be made.

Knowledge of spacecraft separations, magnetic field measurement accuracy, and the form of the current structures sampled (e.g., relative scale size) limits the quality of the method. Despite these conditions of application,

in many regions of the magnetosphere it has been shown to be robust and reliable. A number of studies have applied the method successfully, such as the ring current; the magnetotail current sheet; the magnetopause currents, and field aligned currents; as well as other current structures (e.g., flux tubes). Where time stationarity and other special assumptions can be made, or where the spacecraft configuration is highly irregular or less than four spacecraft are available, the method can still be applied to obtain partial components of the current.

In this chapter, we discuss the performance, adaptability, and lessons learned from multispacecraft techniques, with emphasis on the curlometer technique, and the adaptability of the method. In particular, the application to the new sampling regime offered by the new four-point observations of the MMS mission (which covers a dramatically different spatial regime to that of Cluster), offers a tool able to address open questions on small-scale current structures.

4.2. MULTISPACECRAFT ANALYSIS

4.2.1. The Curlometer

The curlometer method [*Dunlop et al*., 1988] provides all components of the electric current density from measurements taken from four spacecraft, based on the assumption that: $\mathbf{curl(B)} = \mu_0 \mathbf{J}$. Using the individual positions and measured magnetic fields at each spacecraft, the curlometer estimates the average current density in the tetrahedral configuration. This may be done by either estimating linear approximations to the spatial gradients needed for **curl(B)**, or using the linear, integral form of Ampère's law ($\mu_0 \int \mathbf{J}.d\mathbf{s} = \int \mathbf{B}.dl$), which leads to an estimate of the average current density, J_{1ij}, normal to the face 1ij of the tetrahedron (see the right hand-side of Fig. 4.1) from:

$$\mu_0 \langle \mathbf{J} \rangle . \left(\Delta \mathbf{R}_i \times \Delta \mathbf{R}_j \right) = \Delta \mathbf{B}_i . \Delta \mathbf{R}_j - \Delta \mathbf{B}_j . \Delta \mathbf{R}_i ,$$
$$\text{e.g.} \mu_0 < \mathbf{J} >_{123} \left(\Delta \mathbf{R}_{12} \times \Delta \mathbf{R}_{13} \right) = \Delta \mathbf{B}_{12} . \Delta \mathbf{R}_{13} - \Delta \mathbf{B}_{13} . \Delta \mathbf{R}_{12} , \quad (4.2)$$

where here, $\Delta \mathbf{B}_{1i}$, $\Delta \mathbf{R}_{1i}$ have been shortened in notation to $\Delta \mathbf{B}_i$, $\Delta \mathbf{R}_i$, but any reference spacecraft can be used. Three faces of the tetrahedron provide three noncoplanar components of the current, which can then be used to construct a full, average vector current density.

An estimate of the average value of div(**B**) over the volume of the tetrahedron can also be made from $< div(\mathbf{B}) > |\Delta \mathbf{R}_i . \Delta \mathbf{R}_j \times \Delta \mathbf{R}_k| = |\Sigma_{cyclic} \Delta \mathbf{B}_i . \Delta \mathbf{R}_j \times \Delta \mathbf{R}_k|$, which indicates by its value (since div(**B**) = 0) the approximate size of the neglected nonlinear gradients [*Dunlop et al*., 2002; *Robert et al*., 1998; and *Haaland et al*., 2004a], indirectly. The shape and size of the spacecraft configuration compared with the relative orientation and spatial scale of the current structures affect the quality of the linear estimate through the form of the nonlinear gradients in **B**. Usually these may be indirectly monitored by the quality parameter, Q = |div(**B**)|/|**curl(B)**|, although for highly nonregular tetrahedral shapes, the use is less certain. Since div(**B**) should ideally be zero, small values of Q are desirable, and, typically, Q is used only to indicate when the curlometer estimate may be bad. Note, however, that div(**B**) is also calculated from gradients in **B** and, thus, is restricted by the same constraints as the curl calculations. The value of Q therefore can not be used to derive *quantitative* error estimates of the current determination. Finally, measurement errors contribute to the overall uncertainty in the linear approximation of both div(**B**) and **curl(B)**.

In the above equations, $\Delta \mathbf{B}_{ij}$ and $\Delta \mathbf{R}_{ij}$ represent differences in the measured magnetic field and spatial position vectors between spacecraft *i* and *j*, respectively (assumed to be measured simultaneously, so that not only uncertainties in the measured **B** and **R**, but also interspacecraft timing errors affect the estimate). Since the full vector current can be constructed using any three of the four faces of the configuration, there is a redundancy in the calculation (by cycling through the choices of three faces), which can verify the sensitivity of the estimate for each Cartesian component of **J** (thus providing a way to assess uncertainty independently to the estimate of div(**B**), and hence Q). This original form of the curlometer is identical to the process of directly estimating the linear spatial gradients for each current density component (see section 4.2.2), for example, from the dyadic of **B**, but the error handling (and hence relevant quality parameter) is slightly different. In the integral form of the method, the estimate is often self-stabilizing for common current structures such as sheets and tubes.

Although the method can be applied to the measured **B** point by point in time, the nature of the linear approximation suggests a further consideration for the preparation of the input data. If the background field contains strong nonlinear gradients (this is the case for the internal geomagnetic field), then the neglect of these gradients in the linear estimates can imply nonphysical (i.e., not real) currents (the effect is significant in the inner magnetosphere and therefore affects the ring current calculation, and the calculation of FACs at low orbit). Moreover, if the curlometer is applied to a geomagnetic model field (such as the IGRF) in which the current is zero, then implied currents from nonzero values will result from the estimate. This effect was first noted in *Dunlop et al*. [2002] and was pursued more recently by *Grimald et al*. [2012]. The solution is to subtract a zero current model field from the measured magnetic field measurements prior to the application of the curlometer, which is then applied to

the residual measured fields [*Dunlop et al.*, 2015b]. It is of course important that any detrending of the data in this way does not remove any real currents, which may be present (and it is usually found to be sufficient to use a defined model field containing no current), unless different current systems (such as large and small scale) need to be separated, and modeled currents are first subtracted.

A further consideration is that nonregular tetrahedral spacecraft configurations preferentially access some components of the current more accurately than others (depending on alignment, or misalignment, to the dominant current direction and its form). This can be a significant pitfall to consider when sampling large-scale currents at the magnetopause or magnetotail, for example; but it can also be a benefit to the measurement of highly directed currents such as field-aligned currents (FACs) where one face of the tetrahedron formed by the spacecraft can be used to estimate the component of the current that is closest to the FAC direction [*Dunlop et al.*, 2015a].

In general terms, accurate computation of any current requires the spatial configuration to be small compared to the characteristic scale size of current structure to minimize the effect of the nonlinear gradients (i.e., nonmeasured gradients in the current density). This requirement, however, is limited by the effect of the measurement errors in **B** and **R** and by timing errors between spacecraft, which become more significant at smaller spatial scales. Thus, smaller tetrahedral scales require higher absolute accuracy in **B** and **R**, and higher temporal behavior requires higher cadence and accuracy of the measurement times. For the smallest Cluster tetrahedron scales (a few 100 km), measurement uncertainty (~0.1 nT in **B**; a few km for **R** and millisecond timing) was sufficiently low (for accessing minimum currents greater than a few nAm^{-2}) that linearization errors typically dominate the lack of knowledge in the estimates. This is why Q was taken as a reasonable quality indicator. At separations of tens of km (as accessed by the MMS mission [*Burch et al.*, 2016]), the curlometer is likely to be more often in the linear regime where errors due to gradients in the current density are small. On these spatial scales, however, the measurement errors could become significant unless the currents measured are large and therefore it is more relevant that all these measurement errors should be minimized. In fact, it is natural that at Cluster separation scales the curlometer misses small-scale structure and therefore that the estimate will typically be lower than actual currents that have forms varying over the spacecraft configuration. We might expect that on MMS scales the estimated currents will be larger than comparative measurements by Cluster (see section 4.3.2). At the magnetopause or in the magnetotail, for example, the boundary layer will often be much larger than the MMS separation scales so that substructures can be resolved.

The preceding outline represents the key issues revealed from the application of the method to Cluster data, following its use in many regions of near-Earth space since the launch of Cluster (see, for instance, *Dunlop and Eastwood*, [2008], for a review, and *Dunlop et al.* [2016], for a summary of the practical experience gained). In section 4.3 we will illustrate the key pitfalls learned through a selection of these applications. Ready to use implementations of the curlometer method can be obtained from the Cluster Science Archive (https://www.cosmos.esa.int/web/csa/multi-spacecraft), and see the technical note by *Middleton and Masson* [2016].

4.2.2. Other Supporting Techniques: Fewer Than Four Spacecraft

There are a number of alternative methods that have been developed relating to the generalized problem of estimating spatial gradients of **B**, and the mapping of these calculations onto the computation of **curl(B)** [*Chanteur*, 1998; *Harvey*, 1998], as well as other gradient-based methods [e.g., *Shi et al.*, 2005, 2006]. For example, standard methods have been developed based on the use of planar reciprocal vectors [*Vogt et al.*, 2008] and the method of least squares [e.g., *DeKeyser et al.*, 2007], and a full calculation of the magnetic rotation rates (MRA, magnetic rotation analysis), leading to estimates of field-line curvature as well as the current density directly has also been developed [see *Shen and Dunlop*, 2008]. The MRA method can also be readily applied to irregular configurations of three to five spacecraft [*Shen et al.*, 2012a].

Recently, the power of these methods has been demonstrated in situations where less than four point measurements are available, or for severely distorted configurations where three spacecraft remain regular or are aligned to the dominant direction of current density. In general, results are returned only for some components of **J** (for example, three spacecraft may still recover one component normal to the plane of the spacecraft), unless other data sets are used in conjunction with the magnetic field, such as the plasma moments, or where assumptions in the behavior of the currents can be made (e.g., stationarity of the field, known FACs, or force-free structures) such as at low Earth orbit recently covered by the multispacecraft Swarm mission [e.g., *Vogt et al.*, 2009, 2013; *Shen et al.*, 2012a, 2012b; *Ritter and Lühr*, 2013].

One application of the method of *Shen et al.* [2012a] has been applied to the group of three magnetospheric THEMIS spacecraft, which came into a close, three-spacecraft configuration at times when they were providing coverage through the Earth's ring current [*Yang et al.*, 2016]. The left-hand side of Figure 4.2 is taken from *Yang et al.* [2016] to illustrate that the current component normal to the configuration can be readily obtained, but

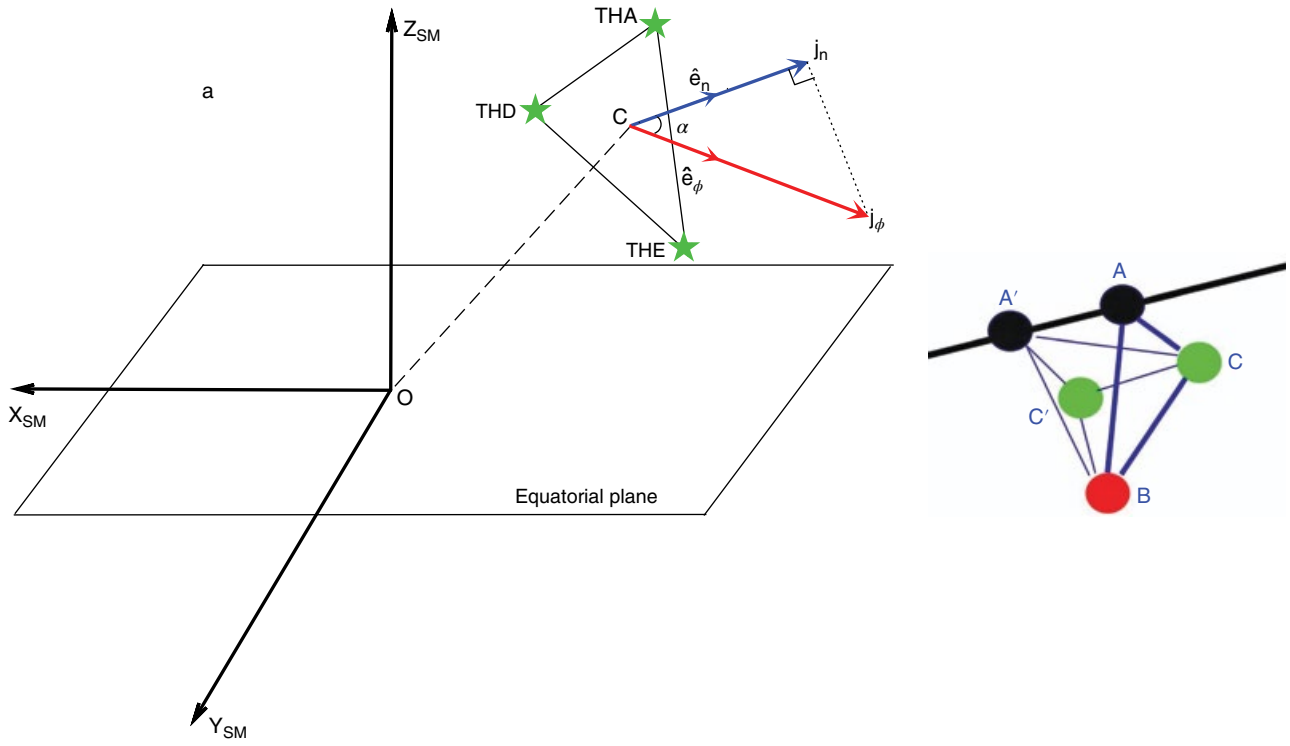

Figure 4.2 (Left) Application of the method of *Shen et al*. [2012a] for the case of three THEMIS spacecraft [from *Yang et al*., 2016]. (Right) Orbit track of the three Swarm spacecraft (A, B, C) when these are grouped closely together. The positions A′, C′ are of these spacecraft a few seconds earlier. When these are combined, giving up to five positions, then the full curlometer can be applied and all components of the current density, *J*, may be recovered (i.e., by using selected configurations of four spatial positions, e.g., A,A′,B,C and using some mean time reference suitable for each configuration). From *Dunlop et al*. [2015a, 2015b].

generally takes some angle relative to the J_ϕ component (in the X, Y plane of the magnetic dipole equator). For large-scale current systems, such as the ring current, where the direction of the main current can be assumed, or for systems of known FACs, where the dominant current is along the known magnetic field direction, this type of application is useful (see section 4.3.3 and 4.3.5).

At low Earth orbit, assumptions of stationarity of the field often can be made, so that positions of the spacecraft at adjacent times can be combined to produce added measurement points, as depicted on the right-hand side of Figure 4.2, allowing the multipoint curlometer to be applied with fewer than four spacecraft. Different configurations of the combined positions are associated with different effective mean times for the measurement. These considerations have been explored in two recent papers [*Dunlop et al*., 2015a, 2015b], which have estimated the full current density at Swarm altitudes using two to four spacecraft positions, and have shown coordinated field-aligned current (FAC) signatures at Cluster and Swarm. In this high field region magnetic residuals are computed by first subtracting a high-resolution internal field model before application of the curlometer.

This is by no means an exhaustive list and the continued usefulness of the curlometer and related techniques in fact lies in flexibility of application and formulation (methodology). Indeed the benchmarking of the method can easily be adapted to new regimes, which we briefly describe below.

4.2.3. Technique Implementation

From equation (4.2), and with reference to the right-hand side of Figure 4.1, it can be seen that the size of the current components perpendicular to each face of the tetrahedron can be found from the terms on the right-hand side of equation (4.2), where the normals to each face (and hence the orientation of these current components) are obtained from $(\Delta\mathbf{R}_i \times \Delta\mathbf{R}_j)/|(\Delta\mathbf{R}_i \times \Delta\mathbf{R}_j)|$, on the left-hand side of equation (4.2). Cartesian components can be found from projections of three of these components onto X, Y, Z coordinates in the usual way. In order to make this

computation from four spacecraft data the time series need to be interpolated onto a common timeline.

4.3. APPLICATIONS

The curlometer method has been successful in view of its wide applicability and robustness and has been successfully applied in many different regions of the Earth's magnetosphere, such as the magnetopause [e.g., *Dunlop et al*., 2002; *Dunlop and Balogh*, 2005; *Haaland et al*., 2004a; *Panov et al*., 2008]; the magnetotail current sheet [e.g., *Runov et al*., 2006; *Nakamura et al*., 2008; *Narita et al*., 2013]; the ring current and inner magnetosphere [e.g., *Vallat et al*., 2005; *Shen et al*., 2014, *Yang et al*., 2016]; field-aligned currents (FAC) [e.g., *Forsyth et al*., 2008; *Shi, et al*., 2010], and other transient signatures [e.g., *Roux, et al*., 2015; *Xiao et al*., 2004; *Shen, et al*., 2008], as well as to structures in the solar wind [e.g., *Eastwood et al*., 2002]. See also Chapters 8 and 11 in this volume.

Many papers have used this technique with Cluster and other multispacecraft combinations. Table 4.1 gives a summary of the typical current density values found previously in the Earth's magnetosphere and solar wind. As noted above, the values are based on the average current density found for typical large-scale structure and as such are likely to miss peaks of small-scale structure within current layers.

4.3.1. The Magnetopause Current Sheet

The magnetopause (MP) is a current sheet forming the boundary between the planetary magnetic field on one side and the shocked solar wind on the other side. It is thus a key region for transfer of mass, momentum, and energy from the solar wind into the magnetosphere. The location of the magnetopause is largely dictated by the balance between the solar wind (primarily dynamic) pressure on one side and the (primarily magnetic) pressure inside the magnetosphere. Due to pressure variations in the solar wind on all timescales, the magnetopause is constantly moving back and forth [e.g., *Sibeck et al*., 1991]. Typical thicknesses for the Earth's magnetopause vary from a few hundred kilometers (a few ion gyro radii) to several thousands of kilometers (*Berchem and Russell*, 1982; *Paschmann et al*., 2005; *Panov et al*., 2008). Typical current densities are of the order 10–100 nAm^{-2}, but small-scale current layers within the magnetopause can have even higher current densities as shown later in this chapter.

An early direct demonstration of the Chapman-Ferraro current (see Fig. 4.3, left, after *Dunlop and Balogh*, [2005]) used a combination of the curlometer and discontinuity analysis (see *Haaland et al*. [2004b] for a review) to probe the magnetopause thickness and orientation for a number of events showing persistence of the MP current; the presence of boundary ripples tied to the current density orientation, and broad scaling of the current density with thickness. The MP was shown to be as thin as 200 km for some crossings (see Fig. 4.3, right, after *Haaland et al*. [2004a]).

4.3.1.1. Example Curlometer Results From the Flank Magnetopause

Figure 4.4 shows Cluster magnetic field measurements and the derived current density and quality criteria from a dusk flank magnetopause (position [–6 16 –7 Re GSE]) crossing on 4 November 2003, about 19:05 UT. The four Cluster spacecraft were flying in a tetrahedron-like formation with a separation distance of around 200 km. At around 19:05 UT, a sharp rotation in the magnetic field was observed, indicating a crossing of the magnetopause current layer from the magnetosphere to the magnetosheath. The actual crossing only took about 17 seconds. Results from plasma moments and triangulation suggested a magnetopause normal velocity of around 35 km/sec, and thus a magnetopause thickness of the order of 600 km.

Structures inside the magnetopause current layer are difficult to resolve with Cluster's 4-sec spin resolution plasma data, but the current (panel e) derived from the high-resolution magnetic field measurements reveal a

Table 4.1 Typical Current Density Values

Feature/Region	Typical values for **J**
Magnetopause currents	~10 $nA\,m^{-2}$ [*Dunlop and Eastwood*, 2008], up to several 100 $nA\,m^{-2}$. See, e.g., *Panov et al.* [2008], Fig. 3.2.
Currents in flux transfer events	~1 $nA\,m^{-2}$ [*Dunlop and Eastwood*, 2008], up to 10 $nA\,m^{-2}$ [*Pu et al.,* 2005].
Current at the cusp boundaries	~20 $nA\,m^{-2}$ [*Dunlop et al*., 2002]. See also Chapter 21 of this volume.
Field aligned currents (FAC) near polar cap	~2 $\mu A\,m^{-2}$ at 500 km altitude and ~20 $nA\,m^{-2}$ at 2.5 R_E altitude [*Dunlop et al.*, 2015a]; See also Chapter 17 of this volume.
Magnetotail current sheet	Up to ~30 $nA\,m^{-2}$ [*Runov et al.,* 2006].
Currents in the plasma sheet boundary layer	~10 $nA\,m^{-2}$ [*Nakamura et al.,* 2004].
Ring current	9–27 $nA\,m^{-2}$ at 4–4.5 R_E [*Zhang et al*., 2011]. See also Chapter 8 of this volume.
Solar wind current sheet	~10 $nA\,m^{-2}$ [*Eastwood et al*., 2002].

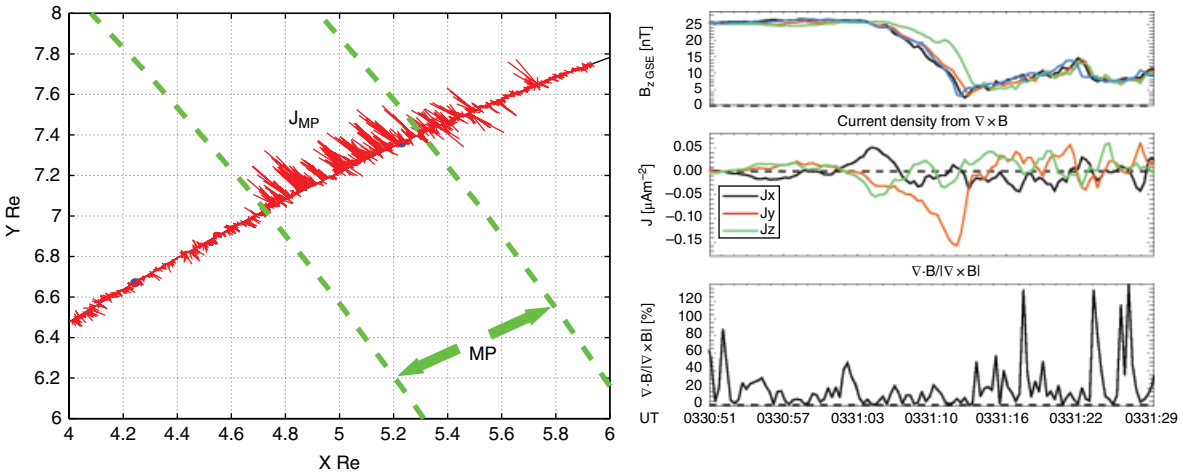

Figure 4.3 (Left) Scan of the curlometer results from the traversal on 26 January 2001, plotted as projections of current orientations as Cluster moves outbound through repeated in-out motions of the MP and into the magnetosheath. (Right) Plot of the current density for a thin magnetopause (2 March 2002) calculated as extending over 200 km, with estimated current densities reaching 150 nAm^{-2}. Here: $\nabla.\mathbf{B} = \mathrm{div}(\mathbf{B})$ and $\nabla \mathrm{x} \mathbf{B} = \mathbf{curl(B)}$.

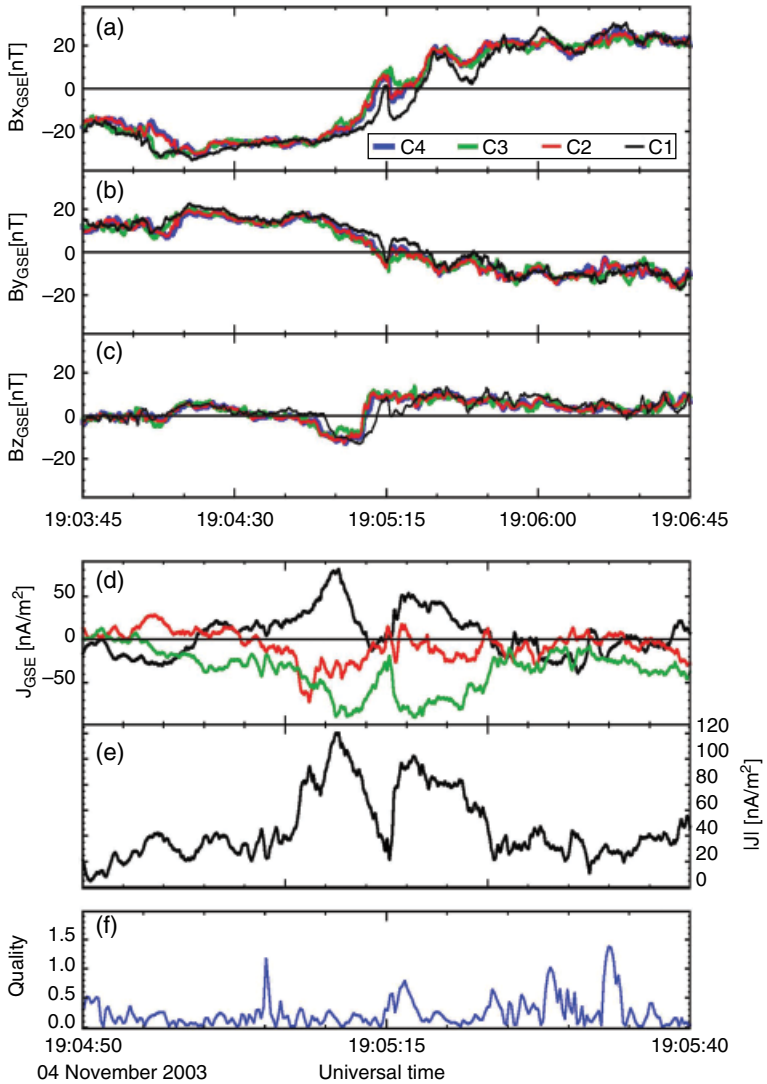

Figure 4.4 Magnetopause current sheet profile during a dusk magnetopause crossing on 4 November 2003. Panels (a), (b), and (c) show high-resolution (at 22.4 vectors/sec) GSE components of the magnetic field; standard Cluster color coding has been used and is indicated in panel (a). Panel (d) shows the individual components of the current (red, X; black, Y, and green, Z). Panel (e) shows the calculated current density, which exhibits a pronounced two-peak structure in this case. Panel (f) shows the quality criteria $Q = |\mathrm{div}(\mathbf{B})|/|\mathbf{curl(B)}|$ discussed in section 4.2.1. After *Haaland et al.* [2014].

layered structure of the current sheet. The magnetospheric side has significant Xgse and Ygse components (black and red lines in panel d), whereas the current on the magnetosheath side has a much stronger Zgse component (green line in panel e). We interpret this as the signature of two adjacent current sheets, with different directions, where each current sheet is only a few ion inertial lengths thick.

Layered current sheets are in no way unique. Similar features were already seen in the first ever reported curlometer results by *Dunlop et al*. [2002], where one of the investigated events from the cusp region showed two distinct peaks in the current density. Layered magnetopause current sheet structures are also often seen in typical kinetic models of the tangential discontinuity magnetopause [e.g., *Roth et al*., 1996].

4.3.1.2. Flank Magnetopause Characteristics

One advantage of the curlometer technique is its robustness and ease of use. *Haaland and Gjerloev* [2013] and *Haaland et al*. [2014] calculated characteristic flank magnetopause properties from more than 1700 Cluster magnetopause traversals during the years 2001–2010. For around 500 crossings, the curlometer technique could be applied to determine peak and average current densities (the other crossings were either partial crossings or had spacecraft separation distances too large for reliable curlometer estimates). Results are shown in Figure 4.5. An interesting result of that study was the persistent dawn-dusk asymmetry observed. *Haaland et al*. [2014] noted that the dusk magnetopause was found to be persistently thinner and with a higher current density than its dawn counterpart, and that, conversely, the typical dawn magnetopause was found to be thicker and with a lower current density. The total current carried is similar for the two flanks. The asymmetry remained if thicknesses were normalized to the local gyro radius. *Haaland et al*. [2014] attributed these results to asymmetries in the magnetosheath and bow-shock geometry, and/or asymmetries in the ring current. These asymmetries would cause a larger magnetic shear and thus higher current density at the dusk-side magnetopause.

4.3.2. Small-Scale Current Structures: MMS Measurements

The small-scale size of the MMS configuration has allowed the detailed structure of many small-scale currents to be revealed for the first time. Figure 4.6 shows an MMS magnetopause crossing (top) compared with a crossing seen by Cluster for similar conditions (studied previously by *Panov et al*. [2006]). For thin MP layers, the scale of the Cluster configuration was much greater than the current layer and as such the estimates of the current densities can be underestimated (often by up to a factor of 2 or 3). The thicknesses of the overall current layers for the MP events in Figure 4.6 are similar and are small compared to the Cluster separations, but large compared to those of MMS; so it is expected that the large-scale current measured at Cluster is underestimated and indeed this shows lower values than those for MMS.

In addition, the sharp spikes in current density seen in the MMS data, associated with smaller scale structures within the current layer, are not seen at all by Cluster. The error estimates from Q are similar in this comparison, but typically are smaller for MMS. In contrast, the errors due to instrumentation are insignificant compared to Q at Cluster since the separation scale is large so that ΔB is much larger than for MMS, as discussed in section 4.2.

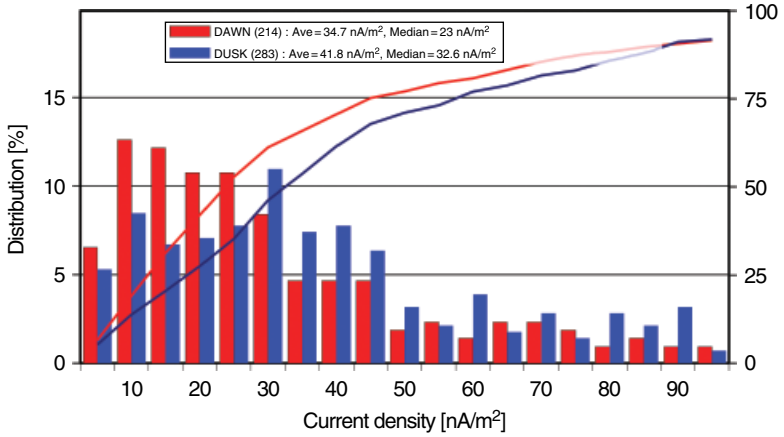

Figure 4.5 (Left) Distribution of magnetopause current densities based on the curlometer results. Each bin in the histograms are 5 nA/m^2 wide. Lines show cumulated values, and refer to the secondary vertical axis at right. Dawn crossings are characterized by lower current densities than their dusk counterparts. After *Haaland et al*. [2014].

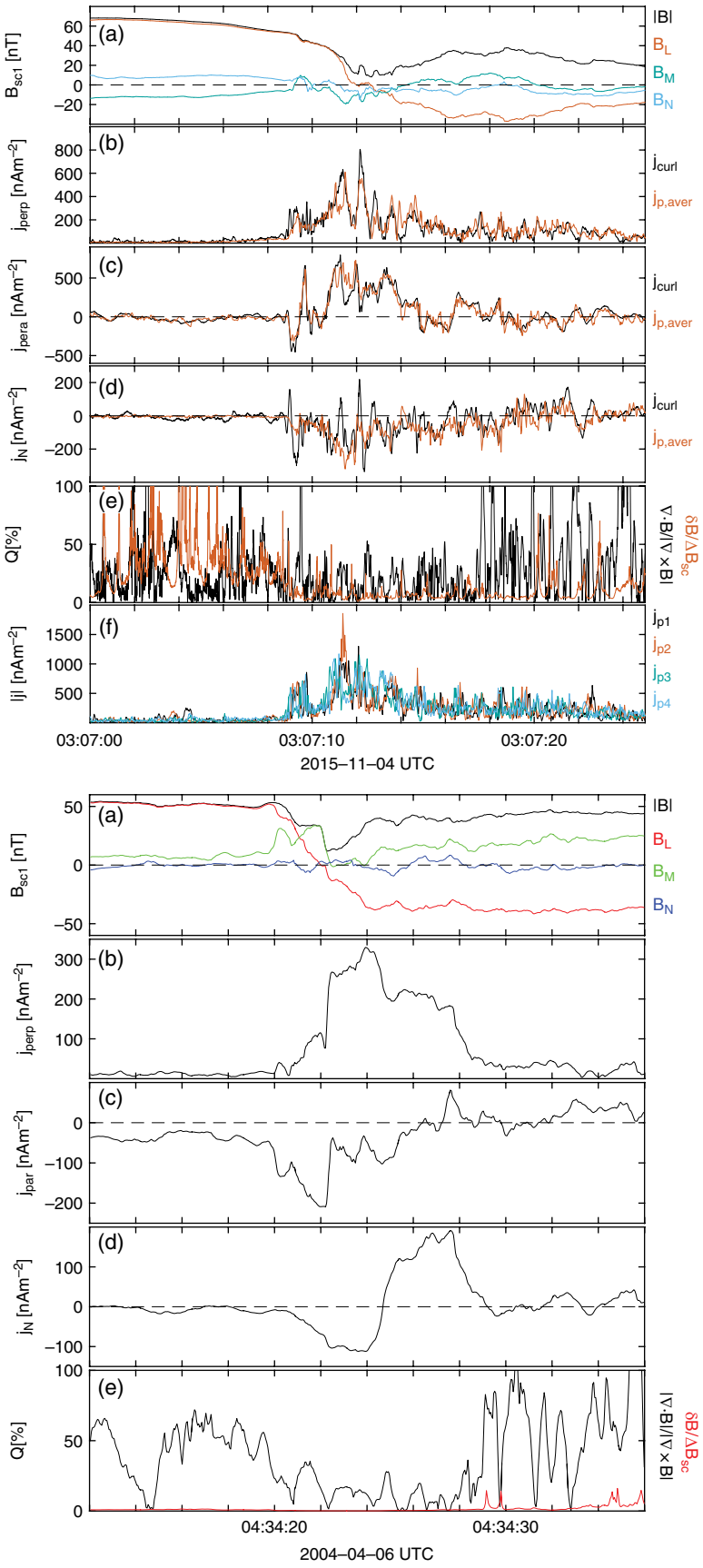

Figure 4.6 Two MP crossings seen by MMS and Cluster for similar thicknesses of ~350 km. (top) MMS data showing: (a) magnetic field in boundary normal coordinates; (b) to (d) the total current density from the curlometer and the mean value of the current density from the four spacecraft ion moments (after equation [4.1]) for the perpendicular, parallel, and boundary normal components; (e) comparison of the quality parameter Q and a crude (upper) estimate of the limit on measurement errors from $\delta B/\Delta B$; (f) the individual total current estimated at each spacecraft from the plasma moments. (Bottom) Cluster data showing (a) to (e) similar parameters to the plots for MMS.
Note: In panels 'e' (top and bottom) Q = |div(**B**)|/|**curl(B)**|

It can also be seen that the individual currents at each spacecraft from the plasma moments (panel (f) for the MMS event) show significant differences, while the mean value over all spacecraft is quite consistent with the curlometer result for all current components (here we have shown the field perpendicular (Chapman-Ferraro current) and parallel (field-aligned current) components and the component normal to the MP, separately). This suggests that there is indeed small-scale structure within the MP current layer and that the dominant current carriers are measured by the plasma moments. The most significant differences between the plasma currents and the curlometer arise in the normal component.

4.3.3. The Terrestrial Ring Current

Another region where the curlometer has been applied is the terrestrial ring current. The ring current (RC) is variable in strength, extends significantly in latitude (–30°–30°) and extends radially from about 2–7 R_E (see Chapter 7 for more details of the RC and other studies of this region). Cluster, for example, generally crosses the ring current every perigee pass. During the earlier phase of the mission, the polar orbit passed normally through the ring current, as was first reported by *Vallat et al.* [2005]. Careful selection of high-quality passes allows a full azimuth scan of the ring current density at all local times (*Zhang et al.* [2011], shown on the left-hand side of Fig. 4.7) and for a limited radial extent (~4–4.5 R_E). By checking the stability of the current density for each pass, the orientation of the Cluster configuration typically allows the azimuthal (ring plane) component, J_ϕ, to be estimated accurately. In order to suppress the effect of nonlinear spatial gradients in the Earth's internal field in this region, the IGRF should be subtracted from the measured data so that estimates of the current density are applied to the field residuals. This requirement has been discussed by *Shen et al.* [2014], who also computed the magnetic field line curvature (using the MRA method) for a number of storm-time events, which also shows the strengthening of the RC with storm activity is reflected in the field-line curvature. MMS also covers the ring current and comparisons may be made with Cluster measurements, but on MMS scales.

A further study has been carried out by *Yang et al.* [2016] using coverage achieved by the three magnetospheric THEMIS spacecraft, while in a close configuration (see left-hand side of Fig. 4.2). The coverage is summarized on the right-hand side of Figure 4.7, where radial coverage is achieved from about 4 up to 12 R_E. The azimuthal coverage is unfortunately limited on the dawn side so that LT trends are not well resolved, but the results show a clear radial profile for the recovery phase of each storm period and resolve the Eastward reverse current on the inner edge of the RC. The eastward to westward ring current boundary is found to be at L = 5, on average, but

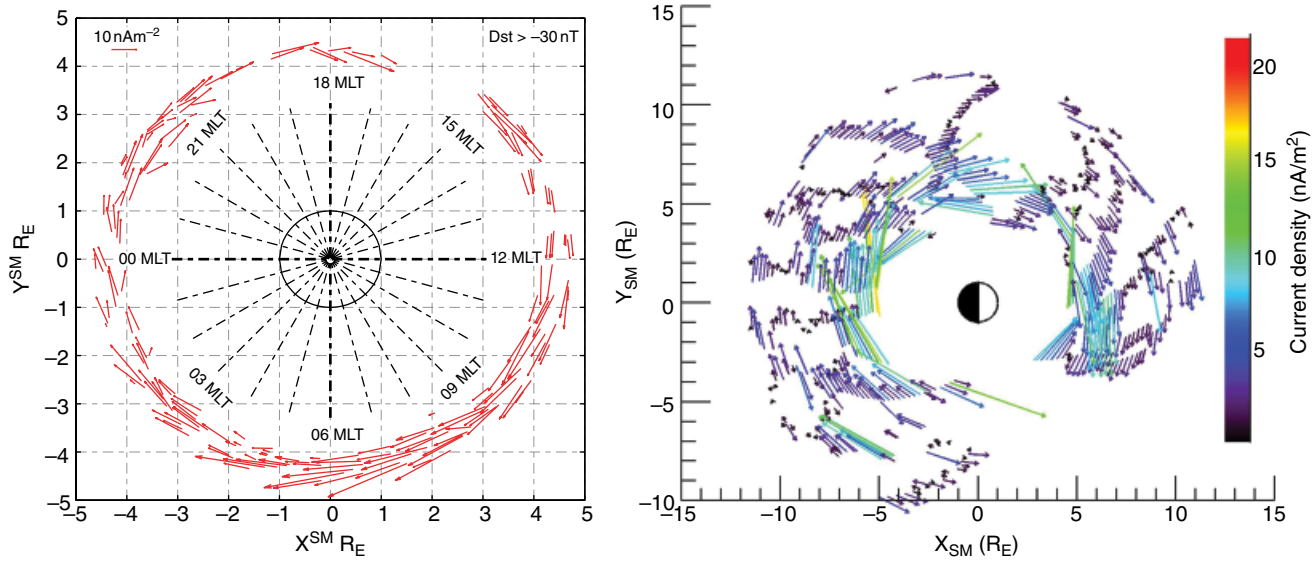

Figure 4.7 (Left) Full azimuth scan (magnetic local time, MLT) of ring current (RC) passes, plotted in solar magnetic (SM) coordinates (dipole aligned), and between –30° to 30° latitude [*Zhang et al.*, 2011]. The length and direction of the vectors represent 10 min averages of the current density obtained from the curlometer. The measurements represent nonstorm (Dst > –30 nT) values of the RC. The RC strength is seen to increase with MLT on the dawn side (03–12 MLT) and is a little suppressed on the dusk side. (Right) THEMIS coverage of the RC for current densities projected into the ring plane and for all storm activities during the recovery phase (i.e., outside the main phase of the storm).

is sensitive to storm activity. There is also a bias to strong storm events near midnight LT.

4.3.4. The Cross-tail Current Sheet

The magnetotail is another region where the curlometer technique has been successfully applied and is reviewed in Chapter 10. Layered current sheet structures similar to those found at the magnetopause have also been observed in the magnetotail. For example, *Runov et al.* [2006] presented a survey of 30 magnetotail current sheet profiles from the first season of Cluster-tail traversals in 2001.

Their study, which was based on the curlometer technique, revealed three distinct tail-current sheet profiles, illustrated in Figure 4.8. Type I current sheet profiles (top panel in Fig 4.8) resemble classic Harris-type current sheet with a symmetric current density in the middle of the neutral sheet (i.e., where the B_Max component of the B-field is zero). Type II current sheets (middle panel) are bifurcated, with two distinct current peaks, one on each side of the neutral sheet and a weaker current in the middle. Finally, type III current sheets are single-peak current sheets, but with the current peak shifted away from the neutral sheet. *Runov et al.* [2006] inferred that layered current sheets were the rule rather than the exception for the magnetotail current sheet. They also noted that type I current sheets were typically narrower (~2000 km) and with a higher peak current density than type II current sheets (~4000 km thickness). Type I current sheets were also found to be more short-lived and transient, possibly because they are more susceptible to various plasma instabilities than the thicker, bifurcated type II current sheets.

4.3.5. Field-Aligned Currents

The curlometer has been applied to a wide number of situations involving FACs, which are covered in detail in Section IV of this volume. As mentioned in section 4.2.2, the technique can be applied to both Cluster sampling at a few to several R_E distances from the Earth, and to low-orbit (400 to several hundred kilometer altitudes) as recently sampled by Swarm (*Dunlop et al.*, 2015b). The technique was applied to a survey of events in the magnetotail [*Shi et al.*, 2010] and to a particular event in the plasma sheet boundary layer [*Cheng et al.*, 2016]. For the latter, the particle and curlometer estimates of current density were shown to agree and be dominated by the

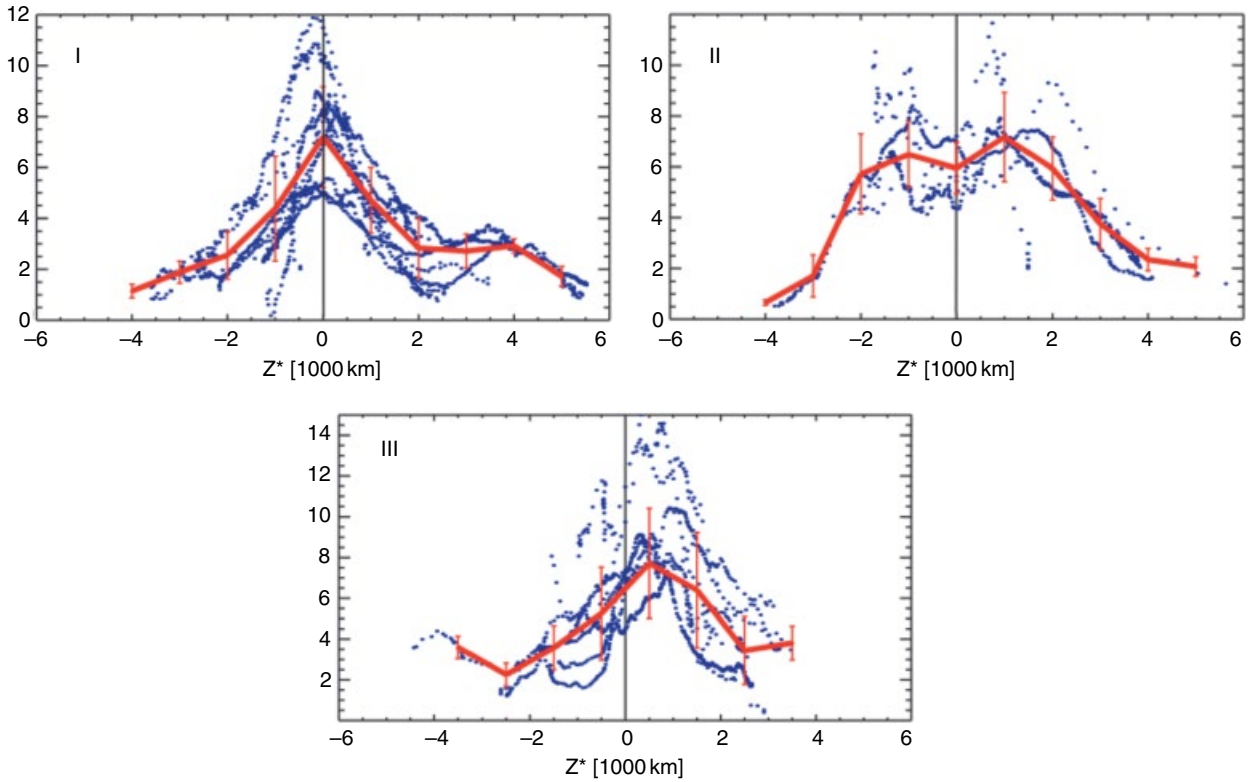

Figure 4.8 Magnetotail current density in μA/m^2 (vertical axes) versus vertical distance from neutral sheet (horizontal axes) individual crossings (blue dots) and ensemble averages (red lines) for three distinctly different current sheet types. From *Runov et al.* [2006].

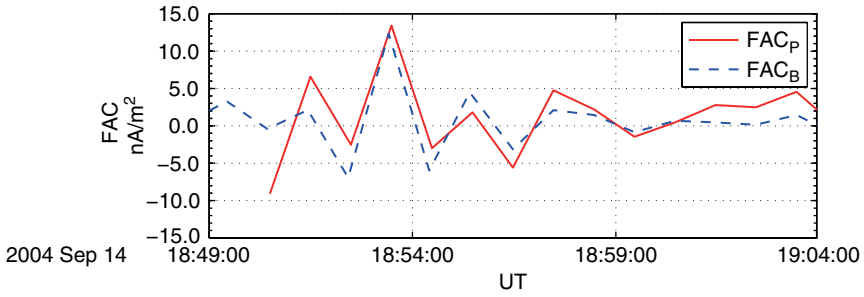

Figure 4.9 The densities of FACs calculated by C3 ions and electron data (FAC_P) and the "curlometer" with the magnetic field data (FAC_B).

electron carriers (see Fig. 4.9). The presence of FACs associated with bursty flows in the magnetotail has also been shown by *Forsyth et al*. [2008].

It is worth mentioning that the curlometer can also measure the currents associated with flux transfer events (FTEs, reconnected flux tubes). These currents are often field aligned in the core of the flux tube, reflecting the force-free nature of the structure. An early demonstration of currents in a large-scale FTE seen by Cluster was recently discussed by *Roux et al*. [2015].

4.4. SUMMARY

Multispacecraft determination of currents, first from Cluster, later from the SWARM and MMS missions, has provided a wealth of new information about current structures in the magnetosphere, and the curlometer has proven to be a reliable and robust tool to determine 3D currents over a wide parameter range in various regions of geospace.

For small-scale current structures, spacecraft separation and configuration, as well as the ability to filter out magnetic field contributions from other sources will necessarily constrain the applicability of the curlometer method [e.g., *Forsyth et al*., 2011]. In these circumstances, direct current determination from particle moments may provide comparative estimates, but the measured distributions require carefully checking to ensure that the calculated moments contain all particles contributing to currents. As noted, such comparisons have been made using Cluster [e.g., the cited *Henderson et al*., 2008: *Petrukovich et al*., 2015, references], but for Cluster this approach has been limited by the availability (ion moments not available from all four spacecraft) and time resolution (Cluster provides particle moments at 4-sec spin resolution) of the plasma measurements. This is a key combination where existing missions like MMS and Swarm (but also proposed missions like THOR and Alfvén) are expected to have plasma instrumentation with the capability for high time-resolution measurements, to provide better estimates and new insight on small-scale current structures. Initial results from MMS [e.g., *Eastwood et al*., 2016] are very promising.

ACKNOWLEDGMENTS

All Cluster data, including software implementation of the curlometer, can be obtained from the ESA Cluster Science Archive (http://www.cosmos.esa.int/web/csa/access). M.W. Dunlop is partly supported by an STFC in-house research grant and is supported by the NSFC grant 41574155. S. Haaland was supported by the Norwegian Research Council under grant BCSS 223252. J.K. Shi is supported by NSFC with No. 41674145. This work is partly supported through the ISSI Team 'from Cluster to MMS'. We thank the International Space Science Institute in Bern, Switzerland, its staff and directors. We also thank the MMS Science Data Center at LASP, University of Colorado, for provision of MMS data.

REFERENCES

Berchem, J., and C. T. Russell (1982), The thickness of the magnetopause current layer: ISEE 1 and 2 observations, *J. Geophys. Res.*, *87*(A4), 2108–2114; doi:10.1029/JA087iA04p02108.

Burch, J. L., T. E. Moore, R. B. Torbert, and B. L. Giles (2016), Magnetospheric multiscale overview and science objectives, *Space Sci. Rev.*, *5*, 1–17; doi:10.1007/s11214-015-0164-9.

Chanteur, G. (1998), Spatial interpolation for four spacecraft: Theory, in *Analysis Methods for Multispacecraft Data*, ISSI Science Report Series, SR-001, 395–418, Kluwer Academic Pub.

Cheng, Z. W., J. C. Zhang, J. K. Shi, L. M. Kistler, M. Dunlop, I. Dandouras, and A. Fazakerley (2016), The particle carriers of field-aligned currents in the Earth's magnetotail during a substorm, *J. Geophys. Res. Space Physics*, *121*, 3058–3068; doi:10.1002/2015JA022071.

De Keyser, J., F. Darrouzet, M. W. Dunlop, and P. M. E. Decreau (2007), Least-squares gradient calculation from multi-point observations of scalar and vector fields: Methodology and applications with Cluster in the plasmasphere, *Ann. Geo.*, *25*, 971–987; doi: 10.5194/angeo-25-971-2007.

Dunlop, M. W., and A. Balogh (2005), Magnetopause current as seen by Cluster, *Ann. Geophys.*, *23*(3), 901–907; doi:10.5194/angeo-23-901-2005.

Dunlop, M. W., and J. P. Eastwood (2008), The Curlometer and other gradient based methods, in *Multi-Spacecraft Analysis Methods Revisited*, edited by G. Paschmann and P. W. Daly,

ISSI ISSI Science Report Series, SR-008, 17–21, Kluwer Academic Pub.

Dunlop, M. W., D. J. Southwood, K.-H. Glassmeier, and F. M. Neubauer (1988), Analysis of multipoint magnetometer data, *Adv. Space Res.*, *8*, 273–277; doi:10.1016/0273-1177(88)90141-X.

Dunlop, M. W., et al. (2002), Four-point Cluster application of magnetic field analysis tools: The Curlometer, *J. Geophys. Res.*, *107*(A11), 1384; doi:10.1029/2001JA005088.

Dunlop, M.W., J.-Y. Yang, Y.-Y. Yang, C. Xiong, H. Lühr, Y. V. Bogdanova, C. Shen, et al. (2015a), Simultaneous field-aligned currents at Swarm and Cluster satellites, *Geophys. Res. Lett.*, *42*, 3683–3691; doi:10.1002/2015GL063738.

Dunlop, M. W., S. Haaland, C.P. Escoubet, and X.-C. Dong (2016), Commentary on accessing 3-D currents in space: Experiences from Cluster, *J. Geophys. Res.*, *121*, 7881–7886; doi:10.1002/2016JA022668.

Dunlop, M. W., Y.-Y. Yang, J-Y. Yang, H. Luhr, C. Shen, N. Olsen, Q.-H. Zhang, et al. (2015b), Multi-spacecraft current estimates at Swarm, *J. Geophys. Res.*, *120*; doi:10.1002/2015JA021707.

Eastwood, J. P., A. Balogh, M. W. Dunlop, and C. W. Smith (2002), Cluster observations of the heliospheric current sheet and an associated magnetic flux rope and comparisons with ACE, *J. Geophys. Res.*, *107*(A11), 1365; doi:10.1029/2001JA009158.

Eastwood, J. P., et al. (2016), Ion-scale secondary flux ropes generated by magnetopause reconnection as resolved by MMS, *Geophys. Res. Lett.*, *43*; doi:10.1002/2016GL068747.

Escoubet, C. P., M. Fehringer, and M. Goldstein (2001), Introduction: The Cluster mission, *Ann. Geophys.*, *19*, 1197–1200; doi10.5194/angeo-19-1197-2001.

Forsyth, C., et al. (2008), Observed tail current systems associated with bursty bulk flows and auroral streamers during a period of multiple substorms, *Ann. Geophys.*, *26*; doi:10.5194/angeo-26-167-2008.

Forsyth, C., M. Lester, A. Fazakerley, C. Owen, and A. Walsh (2011), On the effect of line current width and relative position on the multi-spacecraft curlometer technique, *Planet. Space Science*, *59*, 598–605; doi:10.1016/j.pss.2009.12.007.

Grimald, S., I. Dandouras, P. Robert, and E. Lucek (2012), Study of the applicability of the curlometer technique with the four Cluster spacecraft in regions close to Earth, *Ann. Geophys.*, *30*, 597–611; doi:10.5194/angeo-30-597-2012.

Haaland, S., and J. Gjerloev (2013), On the relation between asymmetries in the ring current and magnetopause current, *J. Geophys. Res.*, *118*, 7593–7604; doi:10.1002/2013JA019345.

Haaland, S., B. O. Sonnerup, M. Dunlop, E. Georgescu, G. Paschmann, B. Klecker, and A. Vaivads (2004a), Orientation and motion of a discontinuity from Cluster curlometer capability: Minimum variance of current density, *Geophys. Res. Letts.*, *31*, L10804–L10804; doi:10.1029/2004GL020001.

Haaland, S., J. Reistad, P. Tenfjord, J. Gjerloev, L. Maes, J. DeKeyser, R. Maggiolo, C. Anekallu, and N. Dorville (2014), Characteristics of the flank magnetopause: Cluster observations, *J. Geophys. Res.*, *119* (11), 9019–9037; doi:10.1002/2014JA020539.

Haaland, S. E., B. Ö. Sonnerup, M. W. Dunlop, A. Balogh, E. Georgescu, H. Hasegawa, B. Klecker, et al. (2004b), Four-spacecraft determination of magnetopause orientation, motion and thickness: comparison with results from single-spacecraft methods, *Ann. Geophys.*, *22*, 1347–1365.

Harvey, C. C. (1998), Spatial gradients and the volumetric tensor, in *Analysis Methods for Multispacecraft Data*, edited by G. Paschmann and P. W. Daly, ISSI Science Report Series, SR-001, 395–418, Kluwer Academic Pub.

Henderson, P. D., et al. (2008), The relationship between *j* and *Pe* in the magnetotail plasma sheet: Cluster observations, *J. Geophys. Res.*, *113*, A07S31; doi:10.1029/2007JA012697; doi:10.1029/2007JA012697.

Kivelson, M., and C. T. Russell (1995), *Introduction to Space Physics*, Cambridge University Press.

Middleton, H. R., and A. Masson (2016), The Curlometer technique: A beginner's guide, *ESA Technical Note*, ESDC-CSA_TN_0001; http://www.cosmos.esa.int/web/csa/multi-spacecraft.

Nakamura, R., W. Baumjohann, M. Fujimoto, Y. Asano, A. Runov, C. Owen, A. Fazakerley, B. Klecker, H. Rème, and E. Lucek (2008), Cluster observations of an ion-scale current sheet in the magnetotail under the presence of a guide field, *J. Geophys. Res.*, 1978–2012, *113*; doi: 10.1029/2007JA012760.

Narita, Y., R. Nakamura, and W. Baumjohann (2013), Cluster as current sheet surveyor in the magnetotail, *Ann. Geophys*, *31*, 1605–1610; doi:10.5194/angeo-31-1605-2013.

Panov, E., J. Büchner, M. Fränz, A. Korth, Y. Khotyaintsev, B. Nikutowski, S. Savin, K.-H. Fornaçon, I. Dandouras, and H. Reme (2006), CLUSTER spacecraft observation of a thin current sheet at the Earth's magnetopause, *Adv. Space Res.*, *37*(7), 1363–1372; doi:10.1029/2006GL026556.

Panov, E. V., J. Buchner, M. Franz, A. Korth, S. P. Savin, H. Reme, and K.-H. Fornacon (2008), High-latitude Earth's magnetopause outside the cusp: Cluster observations, *J. Geophys. Res.*, *113*, A01220; doi:10.1029/2006JA012123.

Paschmann, G., S. Haaland, B. U. Ã. Sonnerup, H. Hasegawa, E. Georgescu, B. Klecker, T. D. Phan, H. Reme, and A. Vaivads (2005), Characteristics of the near-tail dawn magnetopause and boundary layer, *Ann. Geophys.*, *23*, 1481–1497; doi:10.5194/angeo-23-1481-2005.

Petrukovich, A., et al. (2015), Current sheets in the earth magnetotail: Plasma and magnetic field structure with cluster project observations, *Space Sci. Rev.*, *188*, 311–337; doi:10.1007/s11214-014-0126-7.

Ritter, P., and H. Lühr (2013), Determining field-aligned currents with the Swarm constellation mission, *Earth, Planet Space*, *65*, 1285–1294; doi:10.5047/eps.2013.09.006.

Robert, P., M.W. Dunlop, A. Roux, and G. Chanteur (1998), Accuracy of current density determination, in *Analysis Methods for Multispacecraft Data*, edited by G. Paschmann and P. W. Daly, ISSI Science Report Series, SR-001, 395–418, Kluwer Academic Pub.

Roth, M., J. de Keyser, and M. M. Kuznetsova (1996), Vlasov theory of the equilibrium structure of tangential discontinuities in space plasmas, *Space Sci. Rev.*, *76*(3–4), 251–317.

Roux, A., P. Robert, D. Fontaine, O. LeContel, P. Canu, and P. Louarn (2015), What is the nature of magnetosheath FTEs?, *J. Geophys. Res. Space Physices*, *120*(6), 4576–4595; doi:10.1002/2015JA020983.

Runov, A., et al. (2006), Local structure of the magnetotail current sheet: 2001 Cluster observations, *Ann. Geophys.*, *24*, 247–262; doi:10.5194/angeo-24-247-2006.

Russell, C. T., J.G. Luhmann, and R. J. Strangeway (2016). *Space Physics: An Introduction*, Cambridge University Press.

Shen, C., and M. W. Dunlop (2008), Geometric structure analysis of the magnetic field, in *Multi-Spacecraft Analysis Methods Revisited*, edited by G. Paschmann and P.W. Daly, ISSI Science Report Series, SR-008, 27–32, Kluwer Academic Pub.

Shen, C., et al. (2008), Flattened current sheet and its evolution in substorms. *J. Geophys. Res*., *113*, A07S21; doi:10.1029/2007JA012812.

Shen, C., et al. (2014), Direct calculation of the ring current distribution and magnetic structure seen by Cluster during geomagnetic storms, *J. Geophys. Res.*, *119*, 2458–2465; doi:10.1002/2013JA019460.

Shen, C., J. Rong, M. Dunlop, Y. H. Ma, G. Zeng, and Z. X. Liu (2012a), Spatial gradients from irregular, multiple-point spacecraft configurations, *J. Geophys. Res.*, *117*, A11207; doi:10.1029/2012JA018075.

Shen, C., Z. J. Rong, and M. Dunlop (2012b), Determining the full magnetic field gradient from two spacecraft measurements under special constraints, *J. Geophys. Res.*, *117*, A10217; doi:10.1029/2012JA018063.

Shi, J. K., et al. (2010), South-north asymmetry of field-aligned currents in the magnetotail observed by Cluster, *J. Geophys. Res.*, *115*; doi:10.1029/2009JA014446.

Shi, Q. Q., C. Shen, Z. Y. Pu, M. W. Dunlop, Q.-G. Zong, H. Zhang, C. J. Xiao, Z. X. Liu, and A. Balogh, (2005), Dimensional analysis of observed structures using multipoint magnetic field measurements: Application to Cluster *Geophys. Res. Lett*., *32*, CiteID L12105; doi:10.1029/2005GL022454.

Shi, Q. Q., C. Shen, M. W. Dunlop, Z. Y. Pu, Q.-G. Zong, Z. X. Liu, E. Lucek, and A. Balogh (2006), Motion of observed structures calculated from multi-point magnetic field measurements: Application to Cluster, *Geophys. Res. Lett*., *33*, CiteID L08109; doi:10.1029/2005GL025073.

Sibeck, D. G., R. E. Lopez, and E. C. Roelof (1991), Solar wind control of the magnetopause shape, location, and motion, *J. Geophys. Res.*, *96*(A4), 5489–5495; doi:10.1029/90JA02464.

Vallat, C., et al. (2005), First current density measurements in the ring current region using simultaneous multi-spacecraft CLUSTER-FGM data, *Ann. Geophys.*, *23*, 1849–1865; doi:10.5194/angeo-23-1849-2005.

Vogt, J., A. Albert, and O. Marghitu (2009), Analysis of three-spacecraft data using planar reciprocal vectors: methodological framework and spatial gradient estimation, *Ann. Geophys.*, *27*, 3249–3273; doi:10.5194/angeo-27-3249-2009.

Vogt, J., E. Sorbalo, M. He, and A. Blagau (2013), Gradient estimation using configurations of two or three spacecraft, *Ann. Geophys.*, *31*, 1913–1927.

Vogt, J., G. Paschmann, and G. Chanteur (2008), Reciprocal vectors, in *Multi-Spacecraft Analysis Methods Revisited*, edited by G. Paschmann and P. W. Daly, ISSI Science Report Series, SR-008, 27–30, Kluwer Academic Pub.

Xiao, C. J., et al. (2004), Inferring of flux rope orientation with the minimum variance analysis technique, *J. Geophys. Res.*, *109*; doi:10.1029/2004JA010594.

Yang, Y.-Y., C. Shen, M. Dunlop, Z.-J. Rong, X. Li, V. Angelopolous, Z.-Q. Chen, G.-Q. Yan, and Y. Ji (2016), Storm time current distribution in the inner magnetospheric equator: THEMIS observations, *J. Geophys. Res.*, *120*; doi/10.1002/2015JA022145.

Zhang, Q.-H., M. W. Dunlop, M. Lockwood, R. Holme, Y. Kamide, W. Baumjohann, R. -Y. Liu, et al. (2011), The distribution of the ring current: Cluster observations, *Ann. Geo.*, *29*, 1655–1662; doi:10.5194/angeo-29-1655-2011.